THE JOURNAL OF PHYSICAL CHEMISTRY C
A JOURNAL OF THE AMERICAN CHEMICAL SOCIETY

pubs.acs.org/JPCC

Article

Mechanism of Catalytic CO_2 Hydrogenation to Methane and Methanol Using a Bimetallic Cu_3Pd Cluster at a Zirconia Support

Antonija Mravak, Stefan Vajda,* and Vlasta Bonačić-Koutecký*

Cite This: *J. Phys. Chem. C* 2022, 126, 18306−18312

Read Online

ACCESS | Metrics & More | Article Recommendations | Supporting Information

ABSTRACT: For very small nanocluster-based catalysts, the exploration of the influence of the particle size, composition, and support offers precisely variable parameters in a wide material search space to control catalysts' performance. We present the mechanism of the CO_2 methanation reaction on the oxidized bimetallic Cu_3Pd tetramer (Cu_3PdO_2) supported on a zirconia model support represented by $Zr_{12}O_{24}$ based on the energy profile obtained from density functional theory calculations on the reaction of CO_2 and H_2. In order to determine the role of the Pd atom, the performance of Cu_3PdO_2 with monometallic Cu_4O_2 at the same support has been compared. Parallel to methane formation, the alternative path of methanol formation at this catalyst has also been investigated. The results show that the exchange of a single atom in Cu_4 with a single Pd atom improves catalyst/s performance via lowering the barriers associated with hydrogen dissociation steps that occur on the Pd atom. The above-mentioned results suggest that the doping strategy at the level of single atoms can offer a precise control knob for designing new catalysts with desired performance.

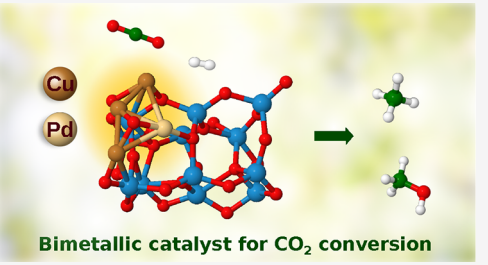

INTRODUCTION

The capture of CO_2 and its catalytic conversion to hydrocarbons, alcohols, and various hydrocarbon derivatives have been of large interest, as an attractive solution for addressing environmental issues by the production of value-added chemicals and fuels. Multiple studies have been reported on the promising performance of copper-based bulk and nanoscale catalysts.[1−13] Recently, catalysts based on small size-selected subnanometer copper clusters and their nanoscale assemblies have been explored extensively both experimentally and theoretically in the conversion of CO_2 into various products, such as methane and methanol.[14−18] Also, the studies should be mentioned which yield other important products such as a diesel fuel surrogate dimethyl ether,[19,20] including catalysts with the copper content. The latter boosts catalyst performance and selectivity toward dimethyl ether.

In order to expand the material search space, cluster-based catalysts allow us to examine the effect of catalytic moiety's size on performance and influence of the composition of the cluster and of the support. In their size and composition, well-defined clusters anchored to the model of a support oxide can be treated by density functional theory (DFT) to gain basic understanding of the function of the catalytic site and the mechanism of the reaction which can ultimately initiate new focused experiments guided by predictions to take various paths. In a joint theoretical and experimental study, we have recently found that subnanometer copper tetramers supported by zirconia are highly efficient for CO_2 hydrogenation and its conversion to methane at high temperature, where catalytic performance was dependent on the cluster size and substrate morphology. DFT simulations on the Cu_4O_2 cluster supported by the $Zr_{12}O_{24}$ subunit ($Cu_4O_2/Zr_{12}O_{24}$) provided a mechanism for CO_2 hydrogenation along the way to conversion to methane, confirming the experimental findings but identifying also methanol formation. These results stimulated us to investigate the possible effect of exchanging a single Cu atom in the cluster with a Pd atom in the tetramer, on the example of Cu_3PdO_2 at $Zr_{12}O_{24}$, on altering performance. In addition to the generally expected effect of an ad-/dopant atom on the electronic structure of the cluster, Pd was chosen also due its well-known role in activation and dissociation of H_2. In other words, the aim of the present study is to optimize the catalytic performance of these copper-based tetramers in CO_2 hydrogenation, by leveraging the proven potential of palladium in the efficient activation of molecular hydrogen, thus providing a control knob on the atomic scale to fine-tune catalyst performance in an atom-by-atom doping fashion. It is to be noted that partially oxidized tetramers were taken into account, based on the reported oxidation states of copper and palladium in mono- and bimetallic clusters studied in situ on the same or similar cluster-based catalysts in

Received: July 12, 2022
Revised: September 14, 2022
Published: October 24, 2022

https://doi.org/10.1021/acs.jpcc.2c04921
J. Phys. Chem. C 2022, 126, 18306−18312

compatible hydrogenation and dehydrogenation reactions.[14−16,18,21−27]

Here, we will first present the mechanism and energy profile of the CO_2 methanation reaction on the bimetallic tetramer (Cu_3PdO_2) at the model zirconia support represented by $Zr_{12}O_{24}$. We will also compare the predicted performance of this mixed tetramer with that of the monometallic Cu_4O_2 cluster at the same support. In addition, we will carry out a parallel investigation of methanol formation on these catalysts, the other major hydrogenation route. This set of exploratory calculations is to support the main hypothesis of this study, namely, to find hints about how a modification of the composition of the catalyst by an exchange of a single metal atom in it shows sufficient advantages in comparison to a monometallic cluster. In this context, detailed comparative investigations of the dominant reaction pathways are being executed as prerequisites for predicting the functioning of the chosen model catalysts that will ultimately lead to computational design of catalysts performing on demand.

■ COMPUTATIONAL METHODS

All the reactive species on the supported bimetallic cluster were optimized employing DFT theory using the Gaussian 16 software package.[28] Calculations of the doublet ground-state structures were performed with the Becke-3-parameter-Lee-Yang-Parr (B3LYP) hybrid functional[29−31] and triple-zeta-valence-plus-polarization (TZVP) basis set[32] for all atoms. In addition, Stuttgart relativistic core potential (ECP)[33] has been used for palladium and zirconium atoms. Structural and electronic properties of both monometallic and bimetallic transition metal clusters can be influenced by dispersion forces.[34] Hence, the Grimme-D3 dispersion correction[35] (GD3) was included to account for the effect of van der Waals (vdW) interactions on the structure and stability of reactive species. To compare energy profiles at bimetallic Cu_3PdO_2 and metallic cluster Cu_4O_2 at the ZrO_2 model support, previous results on the methanation reaction at the supported metallic oxide[18] were recalculated with the addition of the GD3 dispersion. The DFT-computed corrections of relative energies of minima and transition states have been obtained based on Gibbs free energies at 298.15 K and 1 atm as shown in Tables S1 and S2. Activation energies have not been considerably influenced, but relative Gibbs free energies have increased by 0.5−1.5 eV.

■ RESULTS AND DISCUSSION

In this contribution, we first address structural properties of $Cu_3PdO_2/Zr_{12}O_{24}$ in comparison with those of $Cu_4O_2/Zr_{12}O_{24}$ and then attend the reaction pathways for methane and methanol formation, with the goal to determine the role of a single Pd atom and the mechanism involving four necessary hydrogenation steps. In addition, the comparison of results between the monometallic and the bimetallic clusters at the support is of importance because optimization of the composition of the metallic tetramer can be used to improve the performance of the catalyst.

Modeling of the Structural Properties. A model for the bimetallic Cu_3PdO_2 cluster at the support has been investigated by alternatively replacing one by one each of the Cu atoms of the copper tetramer by a Pd atom in a monometallic Cu_4O_2 cluster at the metal oxide support represented by $Zr_{12}O_{24}$ (Figure S1a). Notice that small clusters do not have rigid structures; they can undergo restructuring along the reaction path. Structural fluxionality depends on cluster size, composition, and reaction conditions, as discussed, for example, in the case of copper and palladium clusters of similar size.[24] In our study, the cluster structures are relaxed for every step along the reaction pathway; thus, restructuring/fluxionality is implicitly addressed.

The model for the support $Zr_{12}O_{24}$ has been selected based on previous reactivity studies on the Zr oxide.[36] The lowest energy structure for $Cu_3PdO_2/Zr_{12}O_{24}$ includes the Cu_3Pd tetramer built from CuPd and Cu_2 units which are bound to Zr and O atoms of the support (Figure 1a). This allows the simultaneous formation of the reactive center and connection with the support.

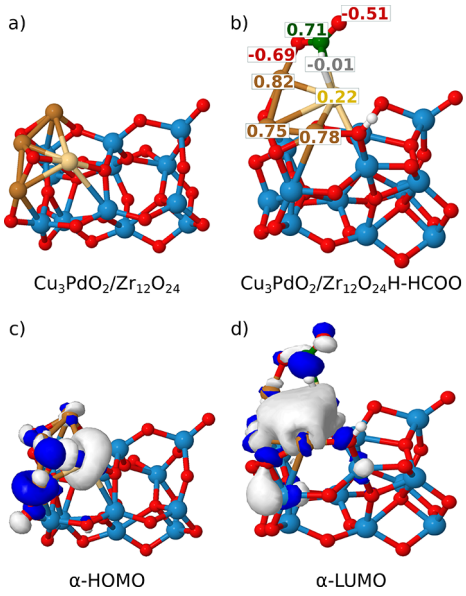

Figure 1. DFT-determined structures for (a) $Cu_3PdO_2/Zr_{12}O_{24}$ and (b) representing binding of structure (a) with CO_2 and H_2 forming $Cu_3PdO_2/Zr_{12}O_{24}H-HCOO$. Values of natural charges are shown in the context of charge transfer within $Cu_3Pd-HCOO$. (c) α-HOMO orbital demonstrating electron delocalization within the oxidized Cu_3Pd cluster. (d) α-LUMO of the structure (b) illustrating electron delocalization within the reactive center Cu_3PdO_2/Zr_4O_5-HCOO. Cu, Pd, O, C, H, and Zr atoms are depicted by brown, yellow, red, green, white, and blue spheres, respectively.

The preferential site for CO_2 binding has been identified at the Cu atom (see isomers in Figure S1b), which was also confirmed by DFT molecular dynamics (DFT-MD) simulations at T = 573.15 K (cf. Figure S2). This temperature was chosen since it is slightly higher than 548.15 K, which is the temperature of CO_2 activation at zirconia-supported Cu_4.[18] Based on natural charge analysis, Pd and Cu atoms have positive values, indicating that the Cu_3Pd cluster is oxidized (Figure 1b). The natural charges of 0.22 for Pd and ~0.8 for Cu atoms reveal polarization of the bimetallic cluster arising from the difference in electronegativity of the Cu and Pd atom (1.9 for Cu vs 2.2 for the Pd atom). The first step of the methanation reaction includes CO_2 activation accompanied by structural adjustment and charge transfer to the CO_2 molecule forming highly reactive CO_2^-.[37] To support these findings, we have examined the charge transfer to adsorbed CO_2 of the structure $Cu_3PdO_2/Zr_{12}O_{24}H-HCOO$ (cf. Figure 1b) and compared it with that of the complementary monometallic

https://doi.org/10.1021/acs.jpcc.2c04921
J. Phys. Chem. C 2022, 126, 18306−18312

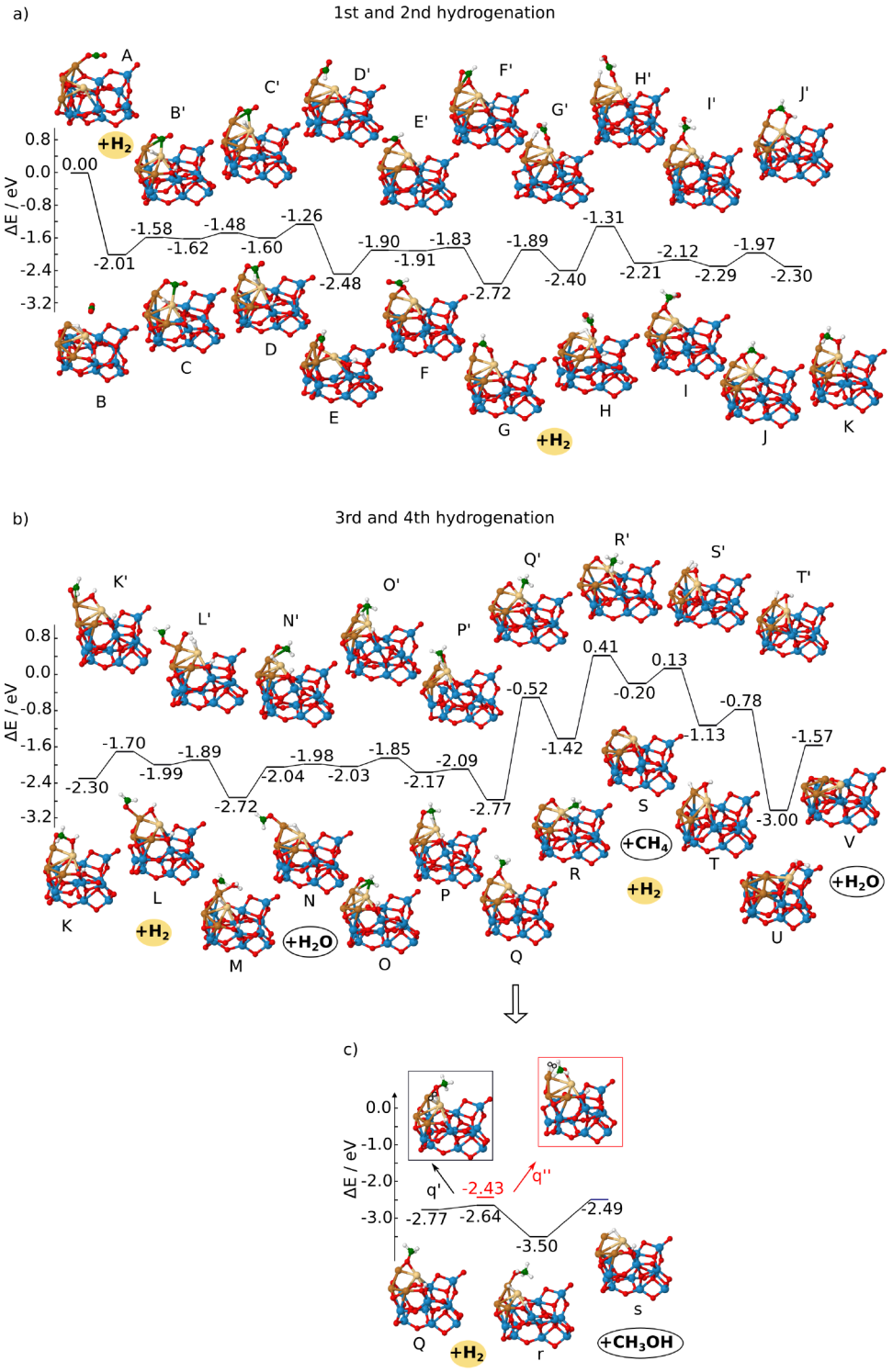

Figure 2. DFT-calculated energy profiles for the CO_2 hydrogenation reaction on the Cu_3PdO_2 cluster supported by $Zr_{12}O_{24}$ including four hydrogenation steps for methane formation in 2(a,b) [first step (A−G), second step (G−L), third (L−S), and fourth (S−V)]. The methanol energy profile is shown in (c). The letters label minima, and letters with primes label transition states.

cluster/support. The electron gain is smaller on the bimetallic (−0.49) versus monometallic oxide cluster at the support (−0.68) confirming gas-phase results from the literature.[38] In addition, the analysis of bond lengths for Pd−C (2.5 Å) versus Cu−C (2.3 Å) supports the fact that higher charge transfer to bound CO_2 occurs within the monometallic than in the bimetallic case (cf. Figure S3).

The highest occupied α molecular orbital (α-HOMO) of $Cu_3PdO_2/Zr_{12}O_{24}$ shows electron delocalization at the oxidized Cu_3Pd cluster (Figure 1c). In order to illustrate charge distribution after H−HCOO binding (Figure 1d), we also demonstrate the lowest unoccupied α molecular orbital (α-LUMO) for the structure from Figure 1b. The electron delocalization is present within −HCOO attached to the cluster and the subunit of the support.

https://doi.org/10.1021/acs.jpcc.2c04921
J. Phys. Chem. C 2022, 126, 18306−18312

A comparison of structural properties between the bimetallic and monometallic cluster at the support illustrates bond length changes within bonding of Pd with O and Zr, and difference in distortion between Cu_3Pd and Cu_4 is also present (cf. Figure S3). The latter may play a central role in exploiting structural changes in the catalytic moiety by the morphology of the underlying support, for example, in structure-sensitive reactions.[4,39−44]

Altogether, described structural properties illustrate the starting point of the reaction pathway including Cu_3PdO_2 at the model of the surface interacting with CO_2 and H_2.

Mechanism of Methane Formation. Conversion of CO_2 to methane by the bimetallic Cu_3PdO_2 cluster at the support involves four hydrogenation steps for which the DFT-calculated energy profile is shown in Figure 2 and in Scheme 1. Analysis of the energy profile provides the mechanism for the methanation reaction.

Scheme 1. Reaction Pathway of CO_2 Hydrogenation at $Cu_3PdO_2/Zr_{12}O_{24}$ Following Figure 2 According to Steps (A−Q), Where Q Is Branching to V and to s[a]

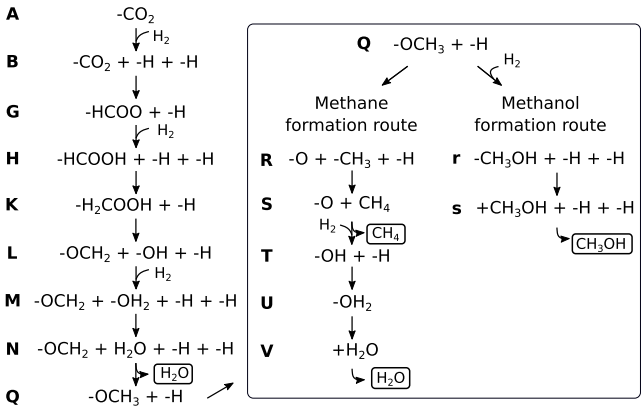

[a]"-" is the symbol for adsorbed species.

At the starting point of the reaction, CO_2 is bound to the Cu atom according to the results of the search for the lowest energy structure. Parallel to the previous investigation of the methanation reaction on monometallic Cu_4O_2 at the support,[18] the formate pathway has been chosen. Therefore, the first hydrogenation step on bimetallic Cu_3PdO_2 at the support shows the formation of −HCOO bound to Cu and Pd atoms. Notice that in order to reach minimum D, which has been addressed in the context of structural properties previously (Figure 1b), relatively small barriers have to be overcome (0.43 and 0.14 eV) between B and D minima. The other steps (E−G) are responsible for additional stabilization of −HCOO. Altogether, the first step is exothermic by −0.71 eV (B → G).

Within the second hydrogenation step, −HCOOH and $-H_2COOH$ species are formed involving two barriers of 0.83 eV (G') and 1.09 eV (H'). After stabilization (Figure 2K), $-H_2COOH$ decomposes into formaldehyde ($-OCH_2$) bound to the Cu atom and hydroxyl (−OH) bound to both Cu and Pd atoms (Figure 2L), overcoming a barrier of 0.6 eV. The mechanism within the second hydrogenation step requires bond breaking resulting in an endothermic pathway (G → L) by 0.73 eV. We investigate also whether the other branches can lower the barriers within the part of the second step. In fact, as shown in Figure S4, hydrogenation at the Pd atom lowers the barriers to 0.34 (e′) and 0.99 eV (f′). These results show that the hydrogenation at the Pd atom can be energetically favorable, suggesting a new role of the Pd atom.

The first H_2O molecule is produced within the third step of hydrogenation overcoming a small activation energy of 0.1 eV. After desorption of H_2O, the methoxy ($-OCH_3$) is created over three steps with barriers of 0.06, 0.18, and 0.08 eV (Figure 2N′−P′). The two barriers corresponding to 2.25 (Figure 2Q′) and 1.83 eV (Figure 2R′) are responsible for breaking the $O-CH_3$ bond and formation of the methane, respectively. Therefore, the third hydrogenation step is endothermic by 1.79 eV (L → S).

The last hydrogenation step includes the formation of the second H_2O molecule over barriers of 0.33 eV (S′) and 0.35 eV (T′), which is exothermic by −1.37 eV (S → V).

In addition, we investigated within the fourth step of the methanation reaction the two more branches. They involve (I) removal of the second water molecule before methane formation (Figure S5) and (II) the fourth hydrogenation taking place at the Pd atom with the aim to determine its role (Figure S6).

The branch (I) was examined to verify if there is an energetically more favorable route for the fourth hydrogenation step. The barrier of 0.37 eV ($\bar{r}'$) has to be overcome for the creation of −OH via hydrogenation at the Cu site. Although a similar barrier value has been found for S′ (Figure 2), the two higher stabilization steps within the branch (I) are present ($\bar{s}$, −2.57 eV and $\bar{u}$, −2.87 eV). The barrier between $\bar{s}$ and $\bar{u}$ is larger ($\bar{s}'$, 1.07 eV), but it is energetically compensated for due to the binding of $-CH_3$ to both Cu and Pd ($\bar{u}$). Despite the large barrier necessary for the formation of CH_4 ($\bar{u}'$), there is sufficient energy available for this endothermic pathway in comparison to that in R′ (cf. Figure 2). Moreover, the branch (I) is energetically accessible and lies below the starting point of the reaction.

The branch (II) serves to examine the energy profile for the pathway using the advantage of binding H_2 at the Pd atom. In fact, starting from the structure S of Figure 2, removal of H_2O is energetically favorable proving an important role of the Pd atom, which involves dissociation of H_2 and stabilization of intermediate steps (cf. u and v of Figure S6).

In summary, only CuPd actively participates in hydrogenation steps. Hydrogen dissociation seems to be well promoted by the Pd atom since it reduces corresponding barriers. Altogether, the mechanism of the CO_2 methanation reaction within four hydrogenation steps involves the formation of −HCOO, −HCOOH, and $-H_2COOH$ intermediate steps. In order to produce CH_4 and H_2O, the breaking of the $-H_2COOH$ into $-OCH_2$ and OH and of $O-CH_3$ into O and $-CH_3$ take place. The latter one is the rate-determining step for the methanation reaction along investigated pathways.

In addition to the formate, we have also considered a reverse water−gas shift reaction (rWGS) pathway, as shown in Figure S7. The route proceeds over the transition state for −COOH formation with a barrier of 1.15 eV and lies below the starting point of the reaction. However, the calculation of the transition state for −OCH formation along this route requires 1.97 eV and is energetically demanding. Overall, the rWGS pathway includes higher energies compared to the formate route.

Mechanism of Methanol Formation. Hydrogenation of methoxy species, which is bound over oxygen to Cu and Pd atoms, yields $Cu-CH_3OH$ (Figure 2c). The transition state can proceed over adsorbed H_2 to either Cu or to the Pd side of

https://doi.org/10.1021/acs.jpcc.2c04921
J. Phys. Chem. C 2022, 126, 18306−18312

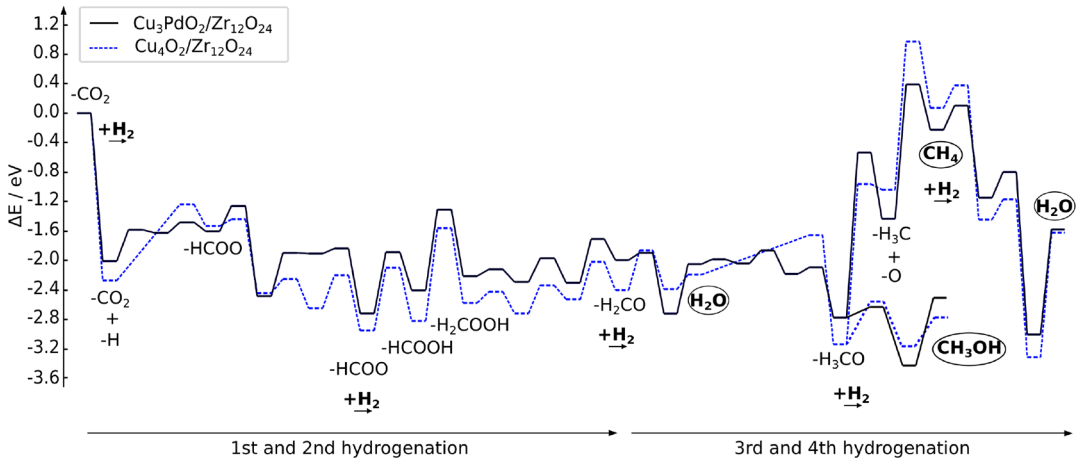

Figure 3. Comparison of DFT energy profiles for four hydrogenation steps of bimetallic Cu_3PdO_2 with the monometallic cluster Cu_4O_2 at the support ($Zr_{12}O_{24}$) involving the two pathways leading to methane and methanol formation.

the methoxy, with barriers of 0.34 and 0.13 eV, respectively. The desorption of methanol from the Cu atom is endothermic by 1.01 eV. The rate-determining step of the methanol pathway is the transition state for the formation of $-H_2COOH$. Altogether, the formation of methanol is energetically favorable on the zirconia-supported bimetallic Cu_3Pd cluster. Our simulations thus suggest an opportunity to convert CO_2 to both methane and methanol depending on the reaction temperature.

Monometallic versus Pd-Doped Bimetallic Oxidized Tetramer Clusters at the Support. Energy profiles of the monometallic and Pd-doped oxidized copper tetramer at the support are compared in Figure 3. Within the first and second hydrogenation steps, both reactions are energetically similar. The first step is exothermic by −0.68 eV for monometallic versus −0.71 eV for bimetallic. The second step is endothermic by 0.55 versus 0.73 eV. Production of the water molecule in the third hydrogenation step requires a higher barrier at Cu_4O_2 (0.54 vs 0.1 eV for bimetallic). This is due to the fact that dissociation of H_2 occurs at the Pd atom. In contrast to the single barrier for the formation of methoxy ($-OCH_3$) at Cu_4O_2 (0.54 eV), three smaller barriers have to be overcome at the bimetallic cluster (0.06, 0.18, and 0.08 eV). Similar barriers at monometallic and bimetallic clusters are present for breaking the $O-CH_3$ bond (2.19 vs 2.25 eV) and formation of the methane (2.02 vs 1.83 eV). This step is more endothermic for Cu_4O_2 (2.5 eV vs 1.79 eV at bimetallic). The barrier for $-CH_3OH$ formation at Cu_4O_2 is 0.56 eV in comparison to smaller barriers at bimetallic species (0.13 eV at Pd or 0.34 eV at Cu). The activation energies required for the formation of second H_2O within the fourth hydrogenation step are similar (0.3 and 0.28 eV vs 0.33 and 0.35 eV). The rate-determining step for both cases is the transition state for breaking of the $O-CH_3$ bond and formation of $Cu-CH_3$ or $Pd-CH_3$. For comparison of energies, see Tables S1−S4.

Overall, the energetic pathways of CO_2 hydrogenation (Figure 3) for both mono- and bimetallic clusters at the zirconia support show that the route for methanol formation is energetically lower compared to the one for the methane formation. This is in line with the earlier theoretical and experimental findings on monometallic Cu_4 at the alumina support,[14] where the methanol was the primary product of the CO_2 hydrogenation at the lower reaction temperatures. On the other hand, methane formation required significantly higher reaction temperatures. Furthermore, experimental investigation of CO_2 hydrogenation at the Cu cluster at the zirconia support[18] revealed that methane is the main product of the reaction, and the methanol signal was not observed at high temperatures. In this context, we conclude that methane versus methanol production is temperature-dependent, regardless of the single atom substitution of the cluster at the support.

In summary, the analysis of the HOMO, LUMO (cf. Figure S8), and charge transfer based on natural charges (Table S5) together with comparison of energy profiles shows the following trends:

(i) In the case of the bimetallic cluster, the CuPd unit presents an interface with the support and has a key role in the hydrogenation steps.

(ii) Hydrogenation steps on the Cu_4O_2 cluster at the support are energetically similar to those occurring at the Cu atom of Cu_3PdO_2. In contrast, the difference between the Pd-doped bimetallic and monometallic cluster is evident when dissociation of H_2 occurs due to the presence of the Pd atom.

(iii) In both cases, the support plays the key role since the metal atoms of tetramers interact directly with Zr and O atoms of the support.

(iv) Production of methane and methanol on both mono- and bimetallic clusters at the zirconia support is temperature-dependent.

(v) In general, the stability of the monometallic cluster at the support is larger than that of the bimetallic one since the charge transfer (cf. Figure S9) from the cluster to the support is larger at the monometallic cluster.

In conclusion, the formate reaction pathway and the obtained mechanism for both monometallic and Pd-doped tetramers at the zirconia support allowed us to identify the synergistic role of the Pd atom in hydrogenation steps. Therefore, the incorporation of palladium in new catalysts might be advantageous, which is also beyond the reaction of interest of the present study, including other reactions where addition or removal of hydrogen takes place. The question which should be addressed in the future is whether an increased number of Pd atoms in a tetramer would improve catalytic performance.

Altogether, very small metallic clusters with extraordinary structural and electronic properties stabilized and affected by

https://doi.org/10.1021/acs.jpcc.2c04921
J. Phys. Chem. C 2022, 126, 18306−18312

the support and doped by other metal atoms show their potential in improving catalyst activity.

CONCLUSIONS

The aim of this study was to computationally explore new ways of tuning catalyst performance down at the atomic level by high-level control of the composition of the catalytic moiety, on the case study of the monometallic copper tetramer and its modification with one of the copper atoms exchanged for a palladium atom yielding the Cu_3Pd bimetallic cluster. Overall, the results show (i) the central role of the CuPd unit in reaction steps; (ii) the influence of the Pd atom on the hydrogenation steps in which it directly participates, demonstrated by lowering the energy barriers along the reaction coordinate; (iii) the key role of the support due to interaction of the tetramers with Zr and O atoms by charge transfer and its redistribution within the different metal atoms in the clusters; (iv) the finding that production of methanol and methane can be influenced by the choice of temperature, and this is independent from the Pd atom substitution; and (v) higher stability of the monometallic than that of the bimetallic cluster evidenced by the larger charge transfer from the cluster to the support. Finally, we conclude that atomic-level doping energetically lowers hydrogenation steps, offering a potential to tailor performance of the catalyst.

ASSOCIATED CONTENT

Supporting Information

The Supporting Information is available free of charge at https://pubs.acs.org/doi/10.1021/acs.jpcc.2c04921.

Tables with values of relative electronic and Gibbs free energies for hydrogenation steps at the bimetallic/support; tables with values of relative electronic energies for hydrogenation steps at the monometallic cluster/support; DFT-calculated isomers of the catalytic complex; results of the DFT-MD calculations of CO_2 binding to the bimetallic/support; comparison of chosen bond lengths; alternative branch for the second hydrogenation step; branches of the energy profile for the methane formation within the fourth hydrogenation step; rWGS pathway at the bimetallic cluster/support; orbitals of selected reaction species; table with charge transfer at the Cu or Pd atom associated with hydrogenation steps for both the bimetallic and monometallic cluster/support; and analysis of natural charges for the bimetallic and monometallic cluster/support (PDF)

AUTHOR INFORMATION

Corresponding Authors

Stefan Vajda − *Department of Nanocatalysis, Czech Academy of Sciences, J. Heyrovský Institute of Physical Chemistry, Prague 8 18223, Czech Republic;* orcid.org/0000-0002-1879-2099; Email: stefan.vajda@jh-inst.cas.cz

Vlasta Bonačić-Koutecký − *Center of Excellence for Science and Technology—Integration of Mediterranean Region (STIM), Faculty of Science, University of Split, Split 21000, Croatia; Interdisciplinary Center for Advanced Science and Technology (ICAST) at University of Split, Split 21000, Croatia; Chemistry Department, Humboldt University of Berlin, Berlin 12489, Germany;* orcid.org/0000-0001-6142-5932; Email: vbk@cms.hu-berlin.de

Author

Antonija Mravak − *Center of Excellence for Science and Technology—Integration of Mediterranean Region (STIM), Faculty of Science, University of Split, Split 21000, Croatia;* orcid.org/0000-0002-1252-7390

Complete contact information is available at: https://pubs.acs.org/10.1021/acs.jpcc.2c04921

Notes

The authors declare no competing financial interest.

ACKNOWLEDGMENTS

V.B.-K. and A.M. acknowledge computational facilities of the HPC computer within the STIM-REI project, Doctoral Study of Biophysics at the University of Split, and thank Professor Miroslav Radman at MedILS and Split-Dalmatia County for support. This research was partially supported by the project STIM-REI, Contract Number: KK.01.1.1.01.0003, and funded by the European Union through the European Regional Development Fund—the Operational Programme Competitiveness and Cohesion 2014−2020 (grant no. KK.01.1.1.01). S.V. acknowledges support from the European Union's Horizon 2020 research and innovation program under grant agreement no. 810310, which corresponds to the J. Heyrovský Chair project ("ERA Chair at J. Heyrovský Institute of Physical Chemistry AS CR—The institutional approach towards ERA"). The funders had no role in the preparation of the article.

REFERENCES

(1) Olah, G. A. Beyond Oil and Gas: The Methanol Economy. *Angew. Chem., Int. Ed.* **2005**, *44*, 2636−2639.

(2) Centi, G.; Perathoner, S. Opportunities and Prospects in the Chemical Recycling of Carbon Dioxide to Fuels. *Catal. Today* **2009**, *148*, 191−205.

(3) Peters, M.; Köhler, B.; Kuckshinrichs, W.; Leitner, W.; Markewitz, P.; Müller, T. E. Chemical Technologies for Exploiting and Recycling Carbon Dioxide into the Value Chain. *ChemSusChem* **2011**, *4*, 1216−1240.

(4) Behrens, M.; Studt, F.; Kasatkin, I.; Kühl, S.; Hävecker, M.; Abild-Pedersen, F.; Zander, S.; Girgsdies, F.; Kurr, P.; Kniep, P.; et al. The Active Site of Methanol Synthesis over $Cu/ZnO/Al_2O_3$ Industrial Catalysts. *Science* **2012**, *336*, 893−897.

(5) Mac Dowell, N.; Fennell, P. S.; Shah, N.; Maitland, G. C. The Role of CO_2 Capture and Utilization in Mitigating Climate Change. *Nat. Clim. Change* **2017**, *7*, 243−249.

(6) Choi, Y. H.; Jang, Y. J.; Park, H.; Kim, W. Y.; Lee, Y. H.; Choi, S. H.; Lee, J. S. Carbon Dioxide Fischer-Tropsch Synthesis: A New Path to Carbon-Neutral Fuels. *Appl. Catal., B* **2017**, *202*, 605−610.

(7) Roy, S.; Cherevotan, A.; Peter, S. C. Thermochemical CO_2 Hydrogenation to Single Carbon Products: Scientific and Technological Challenges. *ACS Energy Lett.* **2018**, *3*, 1938−1966.

(8) Palomino, R. M.; Ramírez, P. J.; Liu, Z.; Hamlyn, R.; Waluyo, I.; Mahapatra, M.; Orozco, I.; Hunt, A.; Simonovis, J. P.; Senanayake, S. D.; et al. Hydrogenation of CO_2 on ZnO/Cu (100) and ZnO/Cu (111) Catalysts: Role of Copper Structure and Metal−Oxide Interface in Methanol Synthesis. *J. Phys. Chem. B* **2018**, *122*, 794−800.

(9) Halder, A.; Kilianová, M.; Yang, B.; Tyo, E. C.; Seifert, S.; Prucek, R.; Panáček, A.; Suchomel, P.; Tomanec, O.; Gosztola, D. J.; et al. Highly Efficient Cu-Decorated Iron Oxide Nanocatalyst for Low Pressure CO_2 Conversion. *Appl. Catal., B* **2018**, *225*, 128−138.

(10) De, S.; Dokania, A.; Ramirez, A.; Gascon, J. Advances in the Design of Heterogeneous Catalysts and Thermocatalytic Processes for CO_2 Utilization. *ACS Catal.* **2020**, *10*, 14147−14185.

(11) Ra, E. C.; Kim, K. Y.; Kim, E. H.; Lee, H.; An, K.; Lee, J. S. Recycling Carbon Dioxide through Catalytic Hydrogenation: Recent

Key Developments and Perspectives. *ACS Catal.* **2020**, *10*, 11318−11345.
(12) Zhong, J.-Q.; Shaikhutdinov, S.; Roldan Cuenya, B. Structural Evolution of Ga−Cu Model Catalysts for CO_2 Hydrogenation Reactions. *J. Phys. Chem. C* **2021**, *125*, 1361−1367.
(13) Simkovičová, K.; Qadir, M. I.; Žilková, N.; Olszówka, J. E.; Sialini, P.; Kvítek, L.; Vajda, Š. Hydrogenation of CO_2 on Nanostructured Cu/FeO_x Catalysts: The Effect of Morphology and Cu Load on Selectivity. *Catalysts* **2022**, *12*, 516.
(14) Liu, C.; Yang, B.; Tyo, E.; Seifert, S.; DeBartolo, J.; von Issendorff, B.; Zapol, P.; Vajda, S.; Curtiss, L. A. Carbon Dioxide Conversion to Methanol over Size-Selected Cu_4 Clusters at Low Pressures. *J. Am. Chem. Soc.* **2015**, *137*, 8676−8679.
(15) Yang, B.; Liu, C.; Halder, A.; Tyo, E. C.; Martinson, A. B.; Seifert, S.; Zapol, P.; Curtiss, L. A.; Vajda, S. Copper Cluster Size Effect in Methanol Synthesis from CO_2. *J. Phys. Chem. C* **2017**, *121*, 10406−10412.
(16) Halder, A.; Kioseoglou, J.; Yang, B.; Kolipaka, K. L.; Seifert, S.; Ilavsky, J.; Pellin, M.; Sowwan, M.; Grammatikopoulos, P.; Vajda, S. Nanoassemblies of Ultrasmall Clusters with Remarkable Activity in Carbon Dioxide Conversion into C1 Fuels. *Nanoscale* **2019**, *11*, 4683−4687.
(17) Yang, B.; Yu, X.; Halder, A.; Zhang, X.; Zhou, X.; Mannie, G. J.; Tyo, E.; Pellin, M. J.; Seifert, S.; Su, D.; et al. Dynamic Interplay between Copper Tetramers and Iron Oxide Boosting CO_2 Conversion to Methanol and Hydrocarbons under Mild Conditions. *ACS Sustain. Chem. Eng.* **2019**, *7*, 14435−14442.
(18) Halder, A.; Lenardi, C.; Timoshenko, J.; Mravak, A.; Yang, B.; Kolipaka, L. K.; Piazzoni, C.; Seifert, S.; Bonačić-Koutecký, V.; Frenkel, A. I.; et al. CO_2 Methanation on Cu-Cluster Decorated Zirconia Supports with Different Morphology: A Combined Experimental In Situ GIXANES/GISAXS, Ex Situ XPS and Theoretical DFT Study. *ACS Catal.* **2021**, *11*, 6210−6224.
(19) Pechenkin, A.; Potemkin, D.; Badmaev, S.; Smirnova, E.; Cherednichenko, K.; Vinokurov, V.; Glotov, A. CO_2 Hydrogenation to Dimethyl Ether over In_2O_3 Catalysts Supported on Aluminosilicate Halloysite Nanotubes. *Green Process. Synth.* **2021**, *10*, 594−605.
(20) Pechenkin, A.; Potemkin, D.; Rubtsova, M.; Snytnikov, P.; Plyusnin, P.; Glotov, A. CuO-In_2O_3 Catalysts Supported on Halloysite Nanotubes for CO_2 Hydrogenation to Dimethyl Ether. *Catalysts* **2021**, *11*, 1151.
(21) Mammen, N.; Spanu, L.; Tyo, E. C.; Yang, B.; Halder, A.; Seifert, S.; Pellin, M. J.; Vajda, S.; Narasimhan, S. Reversing Size-Dependent Trends in the Oxidation of Copper Clusters through Support Effects. *Eur. J. Inorg. Chem.* **2018**, *2018*, 16−22.
(22) Timoshenko, J.; Halder, A.; Yang, B.; Seifert, S.; Pellin, M. J.; Vajda, S.; Frenkel, A. I. Subnanometer Substructures in Nanoassemblies Formed from Clusters under a Reactive Atmosphere Revealed using Machine Learning. *J. Phys. Chem. C* **2018**, *122*, 21686−21693.
(23) Liu, Y.; Marcella, N.; Timoshenko, J.; Halder, A.; Yang, B.; Kolipaka, L.; Pellin, M. J.; Seifert, S.; Vajda, S.; Liu, P.; et al. Mapping XANES Spectra on Structural Descriptors of Copper Oxide Clusters using Supervised Machine Learning. *J. Chem. Phys.* **2019**, *151*, 164201.
(24) Zandkarimi, B.; Sun, G.; Halder, A.; Seifert, S.; Vajda, S.; Sautet, P.; Alexandrova, A. N. Interpreting the Operando XANES of Surface-Supported Subnanometer Clusters: When Fluxionality, Oxidation State, and Size Effect Fight. *J. Phys. Chem. C* **2020**, *124*, 10057−10066.
(25) Halder, A.; Lee, S.; Yang, B.; Pellin, M. J.; Vajda, S.; Li, Z.; Yang, Y.; Farha, O. K.; Hupp, J. T. Structural Reversibility of Cu Doped NU-1000 MOFs under Hydrogenation Conditions. *J. Chem. Phys.* **2020**, *152*, 084703.
(26) Halder, A.; Ha, M.-A.; Zhai, H.; Yang, B.; Pellin, M. J.; Seifert, S.; Alexandrova, A. N.; Vajda, S. Oxidative Dehydrogenation of Cyclohexane by Cu vs Pd Clusters: Selectivity Control by Specific Cluster Dynamics. *ChemCatChem* **2020**, *12*, 1307−1315.
(27) Liu, Y.; Halder, A.; Seifert, S.; Marcella, N.; Vajda, S.; Frenkel, A. I. Probing Active Sites in Cu_xPd_y Cluster Catalysts by Machine-Learning-Assisted X-Ray Absorption Spectroscopy. *ACS Appl. Mater. Interfaces* **2021**, *13*, 53363−53374.
(28) Frisch, M. J.; Trucks, G. W.; Schlegel, H. B.; Scuseria, G. E.; Robb, M. A.; Cheeseman, J. R.; Scalmani, G.; Barone, V.; Petersson, G. A.; Nakatsuji, H.; et al. *Gaussian 16*; Revision A.03; Gaussian Inc.: Wallingford CT, 2016.
(29) Becke, A. D. Density-Functional Exchange-Energy Approximation with Correct Asymptotic Behavior. *Phys. Rev. A* **1988**, *38*, 3098−3100.
(30) Lee, C.; Yang, W.; Parr, R. G. Development of the Colle-Salvetti Correlation-Energy Formula into a Functional of the Electron Density. *Phys. Rev. B* **1988**, *37*, 785−789.
(31) Becke, A. D. Density-Functional Thermochemistry. III. The Role of Exact Exchange. *J. Chem. Phys.* **1993**, *98*, 5648−5652.
(32) Weigend, F.; Ahlrichs, R. Balanced Basis Sets of Split Valence, Triple Zeta Valence and Quadruple Zeta Valence Quality for H to Rn: Design and Assessment of Accuracy. *Phys. Chem. Chem. Phys.* **2005**, *7*, 3297−3305.
(33) Andrae, D.; Häußermann, U.; Dolg, M.; Stoll, H.; Preuß, H. Energy-Adjusted Ab Initio Pseudopotentials for the Second and Third Row Transition Elements. *Theor. Chim. Acta* **1990**, *77*, 123−141.
(34) Luna-Valenzuela, A.; Cabellos, J. L.; Alonso, J. A.; Posada-Amarillas, A. Effects of Van der Waals Interactions on the Structure and Stability of $Cu_{8-x}Pd_x$ (x= 0, 4, 8) Cluster Isomers. *Mater. Today Commun.* **2021**, *26*, 102024.
(35) Grimme, S.; Antony, J.; Ehrlich, S.; Krieg, H. A Consistent and Accurate Ab Initio Parametrization of Density Functional Dispersion Correction (DFT-D) for the 94 Elements H-Pu. *J. Chem. Phys.* **2010**, *132*, 154104.
(36) Nößler, M.; Mitrić, R.; Bonačić-Koutecký, V. Binary Neutral Metal Oxide Clusters with Oxygen Radical Centers for Catalytic Oxidation Reactions: From Cluster Models toward Surfaces. *J. Phys. Chem. C* **2012**, *116*, 11570−11574.
(37) Álvarez, A.; Borges, M.; Corral-Pérez, J. J.; Olcina, J. G.; Hu, L.; Cornu, D.; Huang, R.; Stoian, D.; Urakawa, A. CO_2 Activation over Catalytic Surfaces. *ChemPhysChem* **2017**, *18*, 3135−3141.
(38) Álvarez-García, A.; Flórez, E.; Moreno, A.; Jimenez-Orozco, C. CO_2 Activation on Small Cu-Ni and Cu-Pd Bimetallic Clusters. *Mol. Catal.* **2020**, *484*, 110733.
(39) Goodman, D. W. Ethane Hydrogenolysis over Single Crystals of Nickel: Direct Detection of Structure Sensitivity. *Surf. Sci. Lett.* **1982**, *123*, L679−L685.
(40) Kirlin, P.; Knoezinger, H.; Gates, B. C. Mononuclear, Trinuclear, and Metallic Rhenium Catalysts Supported on Magnesia: Effects of Structure on Catalyst Performance. *J. Phys. Chem.* **1990**, *94*, 8451−8456.
(41) McCrea, K. R.; Somorjai, G. A. SFG-Surface Vibrational Spectroscopy Studies of Structure Sensitivity and Insensitivity in Catalytic Reactions: Cyclohexene Dehydrogenation and Ethylene Hydrogenation on Pt (111) and Pt (100) Crystal Surfaces. *J. Mol. Catal. A: Chem.* **2000**, *163*, 43−53.
(42) Andersson, M.; Abild-Pedersen, F.; Remediakis, I.; Bligaard, T.; Jones, G.; Engbæk, J.; Lytken, O.; Horch, S.; Nielsen, J.; Sehested, J.; et al. Structure Sensitivity of the Methanation Reaction: H_2-Induced CO Dissociation on Nickel Surfaces. *J. Catal.* **2008**, *255*, 6−19.
(43) Van Santen, R. A. Complementary Structure Sensitive and Insensitive Catalytic Relationships. *Acc. Chem. Res.* **2009**, *42*, 57−66.
(44) Goergen, S.; Yin, C.; Yang, M.; Lee, B.; Lee, S.; Wang, C.; Wu, P.; Boucher, M.; Kwon, G.; Seifert, S.; et al. Structure Sensitivity of Oxidative Dehydrogenation of Cyclohexane over FeO_x and Au/Fe_3O_4 Nanocrystals. *ACS Catal.* **2013**, *3*, 529−539.

https://doi.org/10.1021/acs.jpcc.2c04921
J. Phys. Chem. C 2022, 126, 18306−18312